Cross-talk-dependent cortical patterning of Rho GTPases during cell repair

Alison Moe[a,b,†], William Holmes[c,¶,*], Adriana E. Golding[a,b,§], Jessica Zola[b,‖], Zachary T. Swider[a,b], Leah Edelstein-Keshet[d], and William Bement[a,b,e,¶,*]

[a]Program in Cellular and Molecular Biology, [b]Center for Quantitative Cell Imaging, and [e]Department of Integrative Biology, University of Wisconsin-Madison, Madison, WI 53706; [c]Department of Physics and Astronomy, Vanderbilt University, Nashville, TN 37212; [d]Department of Mathematics, University of British Columbia, Vancouver, BC V6T 1Z2, Canada

ABSTRACT **Rho GTPases such as Rho, Rac, and Cdc42 are important regulators of the cortical cytoskeleton in processes including cell division, locomotion, and repair. In these processes, Rho GTPases assume characteristic patterns wherein the active GTPases occupy mutually exclusive "zones" in the cell cortex. During cell wound repair, for example, a Rho zone encircles the wound edge and is in turn encircled by a Cdc42 zone. Here we evaluated the contributions of cross-talk between Rho and Cdc42 to the patterning of their respective zones in wounded *Xenopus* oocytes using experimental manipulations in combination with mathematical modeling. The results show that the position of the Cdc42 zone relative to the Rho zone and relative to the wound edge is controlled by the level of Rho activity. In contrast, the outer boundary of the Rho zone is limited by the level of Cdc42 activity. Models based on positive feedback within zones and negative feedback from Rho to the GEF-GAP Abr to Cdc42 capture some, but not all, of the observed behaviors. We conclude that GTPase zone positioning is controlled at the level of Rho activity and we speculate that the Cdc42 zone or something associated with it limits the spread of Rho activity.**

Monitoring Editor
Daniel Lew
Duke University

Received: Jul 21, 2020
Revised: May 27, 2021
Accepted: Jun 7, 2021

INTRODUCTION

Cells routinely pattern their cortex to provide local information needed to generate cortical structures (Bement *et al.*, 2006). Such structures may be relatively stable, such as cell–cell junctions, or they may be transient, such as yeast buds, cytokinetic apparatus, or protrusions at the leading edge of crawling cells. For both stable (Citi *et al.*, 2014; Arnold *et al.*, 2017; Stephenson *et al.*, 2019) and transient cortical structures (Bement *et al.*, 2006; Pertz, 2010; Bement and von Dassow, 2014; Fritz and Pertz, 2016; Goryachev and Leda, 2017), the Rho GTPases–Rho, Rac and Cdc42–often act as critical patterning mediators. In keeping with this role, active GTPases can assume a variety of cortical patterns including stripes (Bement *et al.*, 2005; Yuce *et al.*, 2005), rings (Benink and Bement, 2005; Zhang *et al.*, 2008; Abreu-Blanco *et al.*, 2014), and patches (Martin *et al.*, 2016). Often, GTPase patterns are inherently complementary with domains of high Rho activity bordering domains of high Cdc42 or Rac activity (Benink and Bement, 2005; Abreu-Blanco *et al.*, 2014; Martin *et al.*, 2016). Because the different GTPases can activate and inactivate different targets, such complementarity permits a high degree of spatial precision in patterning the cortical cytoskeleton, in that targets of one GTPase can be activated (or inactivated) in a given part of the cortex while targets of another are activated (or inactivated) in neighboring regions (Bement and von Dassow, 2014).

Typically, cortical pattern formation unfolds progressively, with initial homogeneity giving rise to shallow, imprecisely positioned GTPase domains, which develop into clearly recognizable patterns, with the positions and boundaries of GTPase domains well defined.

This article was published online ahead of print in MBoC in Press (http://www.molbiolcell.org/cgi/doi/10.1091/mbc.E20-07-0481) on June 16, 2021.

¶Equal contribution.

Current affiliation: †Department of Medicine, Medical College of Wisconsin, Milwaukee, WI 53226; §Section on Integrative Biophysics, Eunice Kennedy Shriver National Institute of Child Health and Human Development, National Institutes of Health, Bethesda, MD 20892; ‖University of North Dakota Medical School, Grand Forks, ND 58202-9037.

*Address correspondence to: William Bement (wmbement@wisc.edu); William Holmes (william.holmes@vanderbilt.edu).

Abbreviations used: CA, constitutively active; DN, dominant negative; PDE, partial differential equation.

However, understanding the logic of such events is challenging, particularly in dynamic cortical patterning, where a given step may reflect multiple inputs, and the inputs themselves typically evolve rapidly in space and time.

Cell repair is a powerful model to understand GTPase interactions during cortical pattern formation (Sonnemann and Bement, 2011; Nakamura *et al.*, 2018). For example, damage to the plasma membrane of *Xenopus* oocytes or embryonic cells elicits the formation of concentric rings of Rho and Cdc42 activity, with active Cdc42 circumscribing active Rho (Benink and Bement, 2005; Clark *et al.*, 2009). These "zones" of GTPase activity are in fact circular waves (Burkel *et al.*, 2012) and they direct the formation of a contractile array based on actin filaments and myosin-2 that is also concentrically organized and which closes around the wound (Bement *et al.*, 1999; Mandato and Bement, 2001). At least some of the wound-induced patterning evident in the amphibian oocyte reflects the participation of Abr, a dual GEF-GAP (Chuang *et al.*, 1995) that is recruited to the Rho zone where it stimulates Rho activity (via its GEF domain) and suppresses Cdc42 activity (via its GAP domain) (Vaughan *et al.*, 2011; Simon *et al.*, 2013; Holmes *et al.*, 2016).

This response to damage is not limited to amphibian cells: local GTPase activation and actin assembly at wound sites has been observed in yeast (Kono *et al.*, 2012), worms (Xu and Chisholm, 2011), flies (Abreu-Blanco *et al.*, 2011, Abreu-Blanco *et al.*, 2014), and mammalian cells (Miyake *et al.*, 2001; Godin *et al.*, 2011; Horn *et al.*, 2017; DeKraker *et al.*, 2019). Additionally, concentric patterning has been observed in wounded *Drosophila* embryonic syncytia (Abreu-Blanco *et al.*, 2011, 2014; Nakamura *et al.*, 2017), *C. elegans* epidermal cells (Taffoni *et al.*, 2020), and is likely a feature of wounded mammalian muscle cells (Lek *et al.*, 2013; Demonbreun *et al.*, 2016; Davenport and Bement, 2016).

Because the patterning process is initiated by the investigator at a defined place and time, and because it has a radial axis of symmetry, analysis of cortical pattern formation during cell repair can be more straightforward than in other systems. Here, we have used the *Xenopus* oocyte repair model to better understand how cortical patterns are organized. Using manipulation of Rho and Cdc42 activity and computational modeling, we provide evidence that Rho activity regulates zone positioning and Cdc42 activity regulates zone boundaries.

RESULTS

A "plateau" in the Rho zone

Following plasma membrane damage in *Xenopus* oocytes, Rho and Cdc42 are activated around the wound and segregate into discrete, concentric zones (Benink and Bement, 2005). We previously quantified this patterning by measuring fluorescence intensity at different positions within each zone and determining the mean of the signal at one or more time points (Benink and Bement, 2005; Vaughan *et al.*, 2014). However, such measurements omit much of the data and make it difficult to capture dynamic features of the response. To overcome this obstacle, we used radial averaging, which incorporates all of the signal around the wound at each time point into the measurements (Supplemental Figure S1A). Radial averaging also makes it possible to visualize features of the wound response that would otherwise be masked, as revealed by comparing line intensity scans from unaveraged to averaged samples (Supplemental Figure S1, B–D).

Figure 1 shows a montage (Figure 1A) of different time points obtained from a time-lapse, confocal movie (Supplemental Movie S1A) of a wounded oocyte expressing probes for active Rho (GFP-rGBD) and active Cdc42 (mCherry-wGBD), a kymograph generated by radial averaging of the same movie (Figure 1B), and individual line-scan time points (Figure 1C) taken from a movie generated from the kymograph (Supplemental Movie S1B; see Supplemental Figure S1). Four new features of the wound response were evident from this analysis. First, while the Rho and Cdc42 zones abut each other after formation, a dark stripe develops between them at ~90–120 s (Figure 1B). This stripe reflects the fact that the Rho zone, rather than being symmetric, typically comprises both a sharp, 1–2 μm-wide peak on the side of the zone facing the wound and a broader, less-intense "plateau" on the side of the zone facing away from the wound (Figure 1C; Supplemental Movie S1B). While the extent of the plateau varied from sample to sample (Figure 1, D–G, D'–G'), they were visible in 91% of the samples analyzed at 120 s postwounding (53/58). Second, while both Rho and Cdc42 activity begins to rise at the same time (approximately 20 s postwounding), Cdc42 activity initially rises more quickly (Figure 1C; Supplemental Movie S1). Third, from the point where it is clearly evident, the rising Rho peak is positioned closer to the wound than the Cdc42 peak (Figure 1C; 00:40; Supplemental Figure S1D; 00:20), and this difference becomes more pronounced over time. Fourth, while the zones represent the most obvious accumulation of GTPase activity, there is a subtle but significant increase in both Rho and Cdc42 activity throughout the entire wound area (Figure 1, B, D, H, and I) that commences immediately after wounding and which persists over the course of the experiment. In other words, not only does GTPase activity rise in the focal areas that define the zones but also there is an overall increase in background Rho and Cdc42 activity postwounding.

Low-level Rho suppression displaces the Cdc42 zone to the wound edge and merges the Rho and Cdc42 zones

In a previous study, the role of Rho and Cdc42 cross-talk on GTPase patterning during repair of *Xenopus* oocytes was assessed via expression of dominant negative (DN) or constitutively active (CA) Rho or Cdc42 (Benink and Bement, 2005). In that study, the DN and CA constructs were expressed at concentrations that resulted in the visibly evident reduction or elevation of the target GTPase in cells prior to wounding. While this approach has the virtue of ensuring that the activity of the target GTPase is indeed changed, it has two drawbacks. First, it runs the risk that any of the observed effects may reflect long-term changes to the cortical architecture, rather than immediate roles for cross-talk in the wound response. Second, in some cases, a given GTPase zone was completely eliminated, which made it impossible to draw conclusions about the potential roles of cross-talk in spatial patterning. For example, expression of DN Cdc42 at levels high enough to reduce prewound Cdc42 activity completely suppressed formation of the Rho zone, precluding assessments about the impact of Cdc42 activity reduction on Rho zone positioning. To avoid these problems, we titered the concentrations of the mutant constructs to find the lowest concentration that produced a cross-talk phenotype while minimally impacting prewound levels of the target GTPase. Additionally, we employed complementary approaches designed to have the same anticipated effect on the target GTPase, but which did not entail the use of mutant GTPases.

To assess the consequences of low-level reduction of Rho activity on the Rho and Cdc42 zones, oocytes were microinjected with either DN Rho mRNA or C3 exotransferase (C3; a bacterial toxin that specifically inactivates Rho; Braun *et al.*, 1989) (see *Materials and Methods*). Under the conditions employed, these manipulations had no significant effect on either the pre- or postwound background of Rho or Cdc42 activity (Supplemental Figure S2), but both

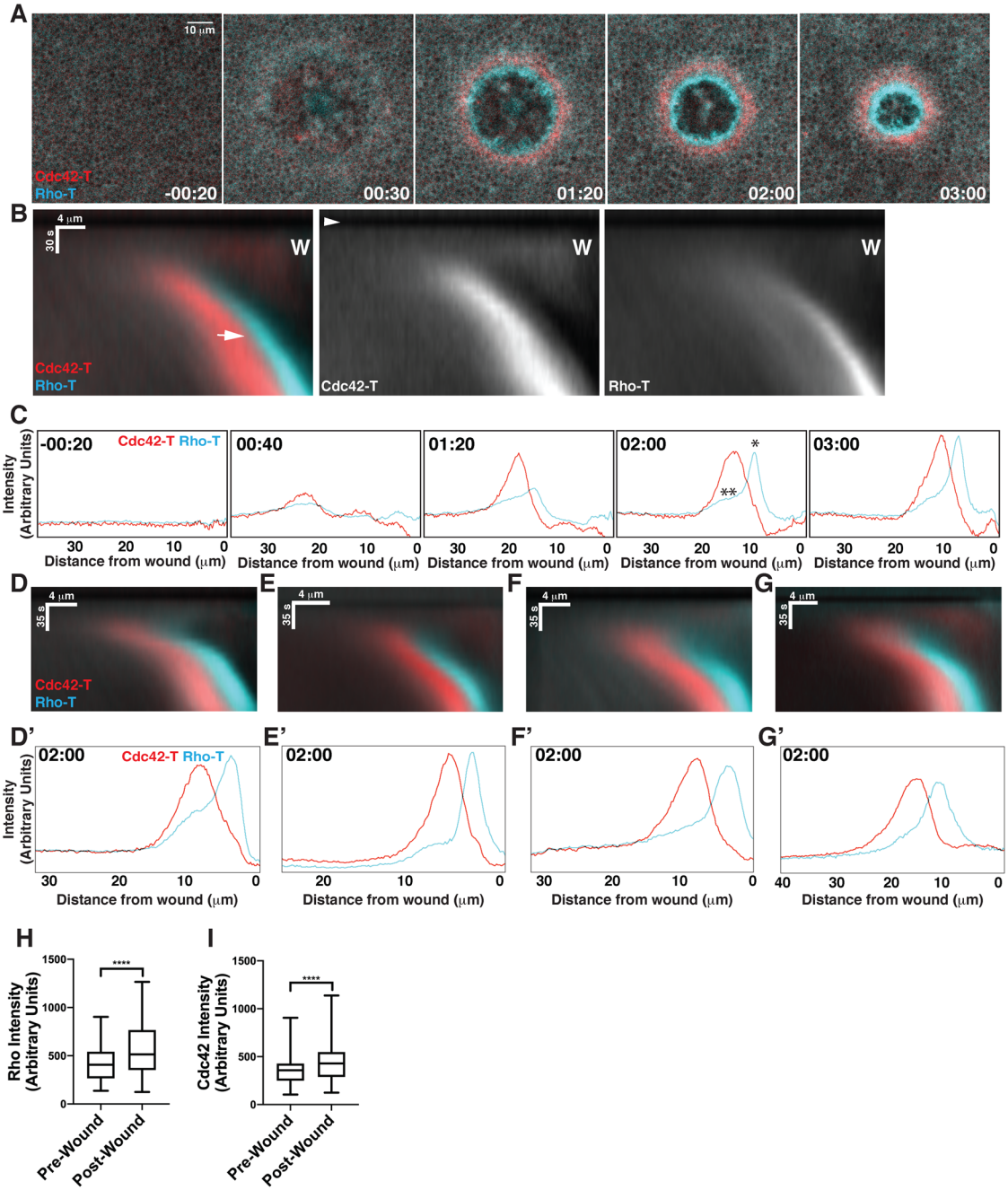

FIGURE 1: Radial averaging reveals a plateau within the Rho activity zone. (A) Montage of individual frames taken from a time-lapse, confocal movie of wounded *Xenopus* oocyte labeled with probes for active Cdc42 (Cdc42-T; red) and active Rho (Rho-T; cyan). The wound is in the center of the field of view and time is in minutes:seconds. See Supplemental Movie S1A. (B) Kymograph generated by radial averaging shown as double label for both active Rho and Cdc42 (left) or single channels showing Cdc42 (middle) or Rho (right). W indicates the position of the wound; the arrowhead (middle panel) shows time of wounding; the arrow (left panel) indicates dark stripe between Rho and Cdc42 zones. (C) Line scan plots derived from the kymograph shown in B (generated as shown in Supplemental Figure S1); wound is on the right. Time is in minutes:seconds; the single asterisk indicates the zone peak; the double asterisk indicates zone plateau. Note also that postwound background is higher than prewound background (compare signal baseline in –00:20 to the other panels) and that Cdc42 zone initially rises more quickly than Rho zone (compare 00:40 to 01:20). See Supplemental Movie S1B. (D-G) Radial average kymographs showing additional examples of control wound repair; the dark stripe is evident in D–F, but not G. (D'-G') Line scan plots from 02:00 postwound from D–G. Note presence of plateau in all samples, including G. (H, I) Quantification of pre- and postwound Rho and Cdc42 activity background signal, respectively. ****$p < 0.0001$; Students *t* test; $n = 139$.

significantly reduced the intensity of the Rho zone (Figure 2, A and B). DN Rho and C3 had inconsistent effects (relative to each other) on the intensity of the Cdc42 zone and on the widths of the Rho and Cdc42 zone (Figure 2, C–E). However, both manipulations nonetheless produced clear GTPase zone positioning phenotypes: First, the Rho and Cdc42 zones merged, as judged by inspection (Figure 2A;

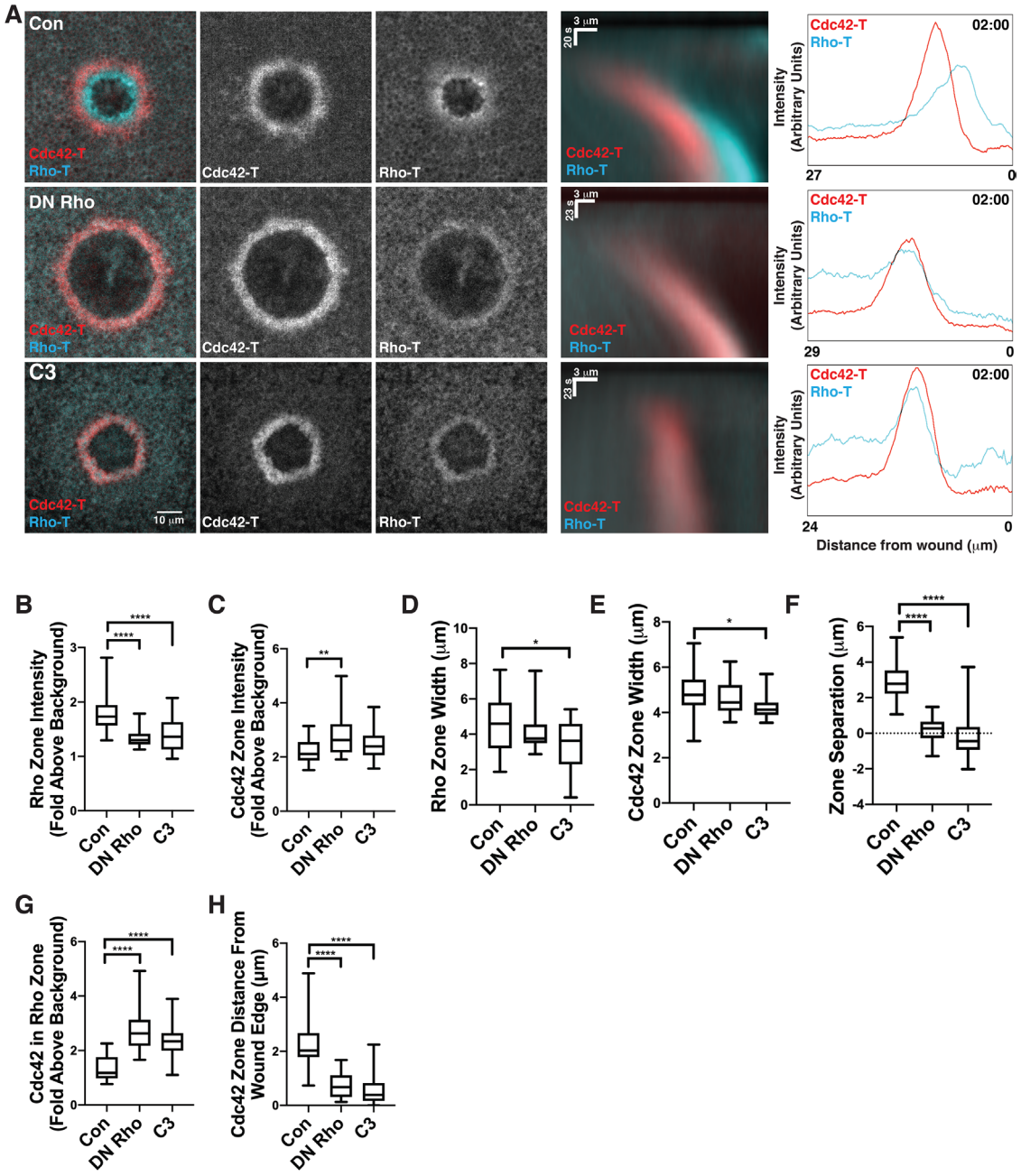

FIGURE 2: Low-level Rho suppression merges Rho and Cdc42 zones and repositions Cdc42 zone. (A) Left: single frames from 2 min postwounding of controls (Con), cells microinjected with DN Rho, or C3 exotransferase (C3) labeled as in Figure 1. Middle: kymographs corresponding to movies from which stills on the right were obtained. Right: line scans corresponding to 2 min point on kymographs in the middle. Note the merging of zones in both experimental groups. (B, C) Quantification of Rho and Cdc42 zone intensity, respectively, at 2 min postwound for control (Con), DN Rho, and C3 exotransferase (C3). (D, E) Quantification of Rho and Cdc42 zone width, respectively, at 2 min postwound for control (Con), DN Rho, and C3 exotransferase (C3). (F) Quantification of GTPase zone separation at 2 min postwound for control (con), DN Rho, and C3 exotransferase (C3). (G) Quantification of Cdc42 signal in Rho zone at 2 min postwound for control (Con), DN Rho, and C3 exotransferase (C3). (H) Quantification of Cdc42 zone distance from wound edge at 2 min postwound for control (Con), DN Rho, and C3 exotransferase (C3). *$p < 0.05$, **$p < 0.01$, ****$p < 0.0001$; one-way ANOVA; Con $n = 35$ cells; DN Rho $n = 19$ cells; C3 $n = 21$ cells.

Supplemental Movie S2A), quantification of zone separation (Figure 2F; Supplemental Movie S2B), and quantification of the level of Cdc42 activity within the Rho zone (Figure 2G). Second, rather than being several micrometers from the wound edge as in controls, DN Rho and C3 resulted in the Cdc42 zone being displaced inward such that it abuts the wound edge (Figure 2, A and H).

Low-level Rho elevation increases separation of the Rho and Cdc42 zones and moves the Cdc42 zone farther from the wound edge

To assess the consequences of low-level elevation of Rho activity on the Rho and Cdc42 zones, oocytes were microinjected with CA Rho (see *Materials and Methods*). As a complementary approach, we

generated a CA Rho-GEF by adding a membrane-targeting signal (a CAAX box) to the isolated catalytic (DHPH) domain of the Rho-GEF Larg (CAAX-Larg). Under the conditions employed, neither CA Rho nor CAAX-Larg elevated prewound or postwound background Rho activity (Supplemental Figure S3). Curiously, rather than increasing Rho zone intensity, these manipulations reduced the intensity of both the Rho and the Cdc42 zones (Figure 3, A–C) while having inconsistent effects on zone width (Figure 3, D and E). Strikingly, both manipulations resulted in a significant increase in the separation of the two zones as judged by inspection (Figure 3A; Supplemental Movie S3A), quantification of zone separation (Figure 3F; Supplemental Movie S3B), and quantification of the level of Cdc42 activity within the Rho zone (Figure 3G). Further, both manipulations significantly increased the distance of the Cdc42 zone from the wound border (Figure 3H). In other words, low-level elevation of Rho activity produced the opposite effect on zone positioning as that produced by low-level reduction of Rho activity.

Low-level Rho elevation broadens and dilutes the Abr zone

Previous work showed that the dual GEF-GAP Abr is an important participant in GTPase patterning during wound repair: Abr, a Rho GEF and Cdc42 GAP (Chuang *et al.*, 1995), is targeted to the same general region as active Rho around wounds, where it promotes both Rho activation and Cdc42 inactivation (Vaughan *et al.*, 2011). Further, this recruitment is dependent on Rho activation in that suppression of Rho activation prevents Abr recruitment to wounds, while ectopic Rho activation in the absence of wounding results in Abr recruitment to the plasma membrane (Vaughan *et al.*, 2011). Thus, one potential explanation of low-level Rho elevation-induced effects is that this manipulation alters the distribution of Abr. To test this hypothesis, oocytes expressing 3XGFP-Abr (Vaughan *et al.*, 2011) were wounded in the absence or presence of CA Rho. Under the conditions employed, CA Rho did not increase either pre- or postwound levels of Abr background (Supplemental Figure S4). However, CA Rho nonetheless produced three clear phenotypes: first, the Abr zone was significantly broader in CA Rho expressing samples than controls (Figure 4, A and B). Second, the intensity of the Abr zone was reduced in CA Rho expressing samples relative to controls (Figure 4, A and C). Third, consistent with the results in Figure 3, CA Rho expression resulted in a significant increase in the separation of the Cdc42 and Abr zone peaks (Figure 4D). Thus, low-level elevation of Rho activity results in a redistribution of Abr.

We sought to conduct similar experiments using CAAX-Larg. However, this effort failed: we were unable to achieve a reliable combination of CAAX-Larg and 3XGFP-Abr expression that did not produce gross elevation of background Rho activity levels, likely because of the combinatorial effects of the Rho GEF activity of Abr and CAAX-Larg.

Low-level Cdc42 suppression results in spreading of the Rho zone

Previous work showed that expression of DN Cdc42 sufficient to visibly reduce prewound levels of Cdc42 activity eliminates both the Cdc42 and the Rho zones (Benink and Bement, 2005). Reducing the amount of DN Cdc42 expression produced phenotypes that varied both between and within different batches of cells. A control and examples of three different phenotypes from the same experiment are shown in Supplemental Figure S5A. Depending on the cell in question, DN Cdc42 reduced Cdc42 zone intensity while having no effect on Rho zone intensity (example 1), reduced both Rho and Cdc42 zone intensity (example 2), or eliminated both Rho and Cdc42 zones (example 3). Further reduction of DN Cdc42 expression resulted in samples where neither Rho nor Cdc42 zones were impacted; further increasing them resulted in samples with no Rho or Cdc42 zones at all.

As an alternative to DN Cdc42, we devised two approaches based on the GAP domain of Chimaerin, a GAP for Rac and Cdc42 (Ahmed *et al.*, 1994). In the first approach, the catalytic domain of Chimaerin was fused to a CAAX box (CAAX-Chim) to target it to the plasma membrane, as described above for the CAAX-Larg construct (Supplemental Figure S5B). In the second approach, the catalytic domain of Chimaerin was fused to the C2 domain of protein kinase Cβ (PKCβ; Supplemental Figure S5C). The C2 domain of PKCβ binds to phosphatidylserine, but only on elevation of calcium (Luo and Weinstein, 1993). We previously showed that fusion of the PKCβ C2 domain with fluorescent proteins provides a sensitive reporter for plasma membrane-proximal calcium elevation in wounded cells (Clark *et al.*, 2009) and that it tracks the region of elevated calcium and the Cdc42 zone in wounded oocytes (Davenport *et al.*, 2016). Expression of C2-fluorescent protein fusions has no detectable effect on the healing process (Clark *et al.*, 2009) and, of most interest here, because such constructs are cytosolic prior to wounding but are then specifically recruited to the wound (Supplemental Figure S5D), they provide an opportunity to manipulate the Cdc42 zone in a time-resolved manner.

Under the conditions employed, CAAX-Chim, but not C2-Chim, significantly elevated the prewound and postwound background levels of Rho or Cdc42 activity (Supplemental Figure S5, E–H), and CAAX-Chim reduced the intensity of the Rho zone while C2-Chim elevated it (Figure 5B). However, as designed, both reduced the intensity of the Cdc42 zone (Figure 5C). Both also produced patterning effects on the Rho zone, namely, they expanded the outer boundary of the Rho zone as determined by inspection (Figure 5A; Supplemental Movie S5A and S5B) and by quantification of either the Rho zone width (Figure 5D) or the width of the peak of the Rho zone (Supplemental Figure S5I). The broadening of the Rho zone appeared to be accompanied by an increasing sloppiness of the Rho zone peak, such that its edges appeared much less well defined than controls (Figure 5A). To quantify this effect, the variance of the zone peak width was compared between controls and cells expressing CAAX-Chim or C2-Chim (see *Materials and Methods*). The expression of CAAX-Chim or C2-Chim resulted in a significant increase in the variance of the zone peak width relative to controls (Figure 5I).

Low-level Cdc42 elevation narrows the Rho zone

Finally, to determine the consequences of modestly elevating Cdc42 activity, CA Cdc42 was expressed at low levels (Golding *et al.*, 2019). We were unable to find a concentration that both produced patterning phenotypes and failed to elevate background levels of Cdc42 activity. We therefore used the lowest concentration of CA Cdc42 capable of producing a Rho zone phenotype (see *Materials and Methods*), which had no effect on the prewound background levels of Rho but elevated the postwound background levels of Rho and the pre- and postwound background levels of Cdc42 (Supplemental Figure S6). Similar to the consequences of CA Rho expression, CA Cdc42 reduced the intensity of both the Rho and the Cdc42 zones (Figure 6, A–C); however, it should be noted that this conclusion is complicated by the fact that the CA Cdc42 elevated the background levels of Cdc42 activity, meaning that the zone intensity reduction reflects, at least in part, elevated background. CA Cdc42 also significantly broadened the Cdc42 zone (Figure 6, A and E; Supplemental Movie S6A and S6B). The broadening was accompanied by a reduction in the amount of Rho activity in the Cdc42

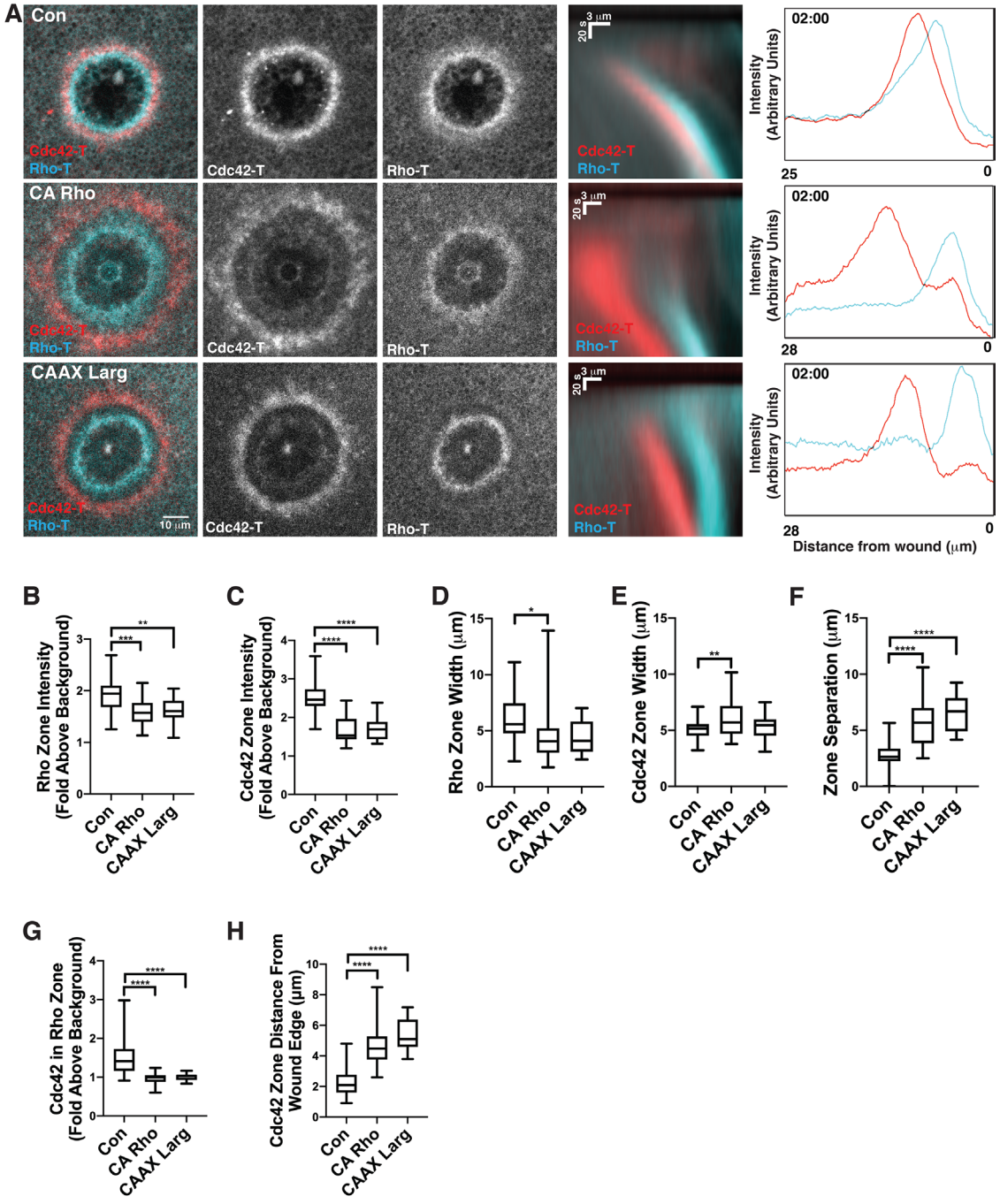

FIGURE 3: Low-level Rho elevation separates Rho and Cdc42 zones and displaces the Cdc42 zone from the wound edge. (A) Left: single frames from 2 min postwounding of controls (Con), cells microinjected with CA Rho or the plasma membrane-targeted Rho GEF domain from Larg (CAAX-Larg) labeled as in Figure 1. Middle: kymographs corresponding to movies from which stills on the right were obtained. Right: line scans corresponding to 2 min point on kymographs in the middle. Note separation of zones in both experimental groups. (B, C) Quantification of Rho and Cdc42 zone intensity, respectively, at 2 min postwound for control (Con), CA Rho, and plasma membrane-targeted Rho GEF domain from Larg (CAAX-Larg). (D, E) Quantification of Rho and Cdc42 zone width, respectively, at 2 min postwound for control (Con), CA Rho, and plasma membrane-targeted Rho GEF domain from Larg (CAAX-Larg). (F) Quantification of GTPase zone separation at 2 min postwound for control (Con), CA Rho, and plasma membrane-targeted Rho GEF domain from Larg (CAAX-Larg). (G) Quantification of Cdc42 signal in Rho zone at 2 min postwound for control (Con), CA Rho, and plasma membrane-targeted Rho GEF domain from Larg (CAAX-Larg). (H) Quantification of Cdc42 zone distance from wound edge at 2 min postwound for control (Con), CA Rho, and plasma membrane-targeted Rho GEF domain from Larg (CAAX-Larg). *$p < 0.05$, **$p < 0.01$, ***$p < 0.005$, ****$p < 0.0001$; one-way ANOVA; Con $n = 35$ cells; CA Rho $n = 23$ cells; CAAX-Larg $n = 23$ cells.

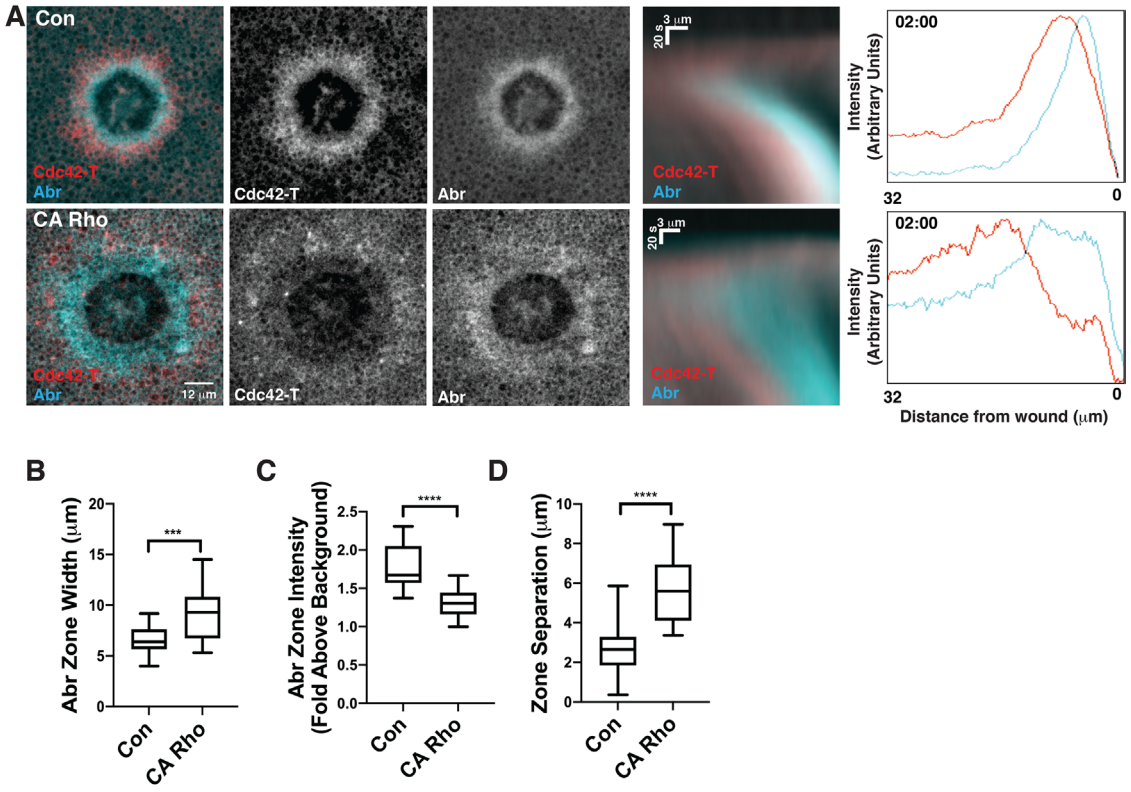

FIGURE 4: Low-level Rho elevation spreads and dilutes the Abr zone. (A) Left: single frames from 2 min postwounding of active Cdc42 (Cdc42-T; red) and Abr-3XGFP (Abr; cyan) in controls (Con), or cells microinjected with CA Rho. Middle: kymographs corresponding to movies from which stills on the right were obtained. Right: line scans corresponding to 2 min point on kymographs in the middle. Note broadening and dilution of Abr signal in the presence of CA Rho. (B) Quantification of Abr zone width at 2 min postwound for control (Con) and CA Rho. (C) Quantification of Abr zone intensity at 2 min postwound for control (Con) and CA Rho. (D) Quantification of Cdc42 and Abr zone separation at 2 min postwound for control (Con) and CA Rho. ***$p < 0.005$, ****$p < 0.0001$; one-way ANOVA; Con $n = 22$ cells; CA Rho $n = 14$ cells.

zone (Figure 6G) which, again, is subject to the caveat pointed out above, and a nonsignificant reduction in the width of the Rho zone (Figure 6D). However, inspection of the Rho zone in en face images and in radially averaged line scans indicated that the expansion of the Cdc42 zone was accompanied by a broadening of the Rho zone plateau and a narrowing of the Rho zone peak (Figure 6A). We therefore quantified the width of the Rho zone at three-quarter height. This measurement revsealed a significant narrowing of the Rho zone peak relative to controls (Figure 6H).

Disruption of the spatial organization of the two zones slows wound closure

While the focus of this study was on patterning, we noticed that the various manipulations that changed the spatial organization of the two zones appeared to impact the speed of closure, as judged by the forward displacement of the Rho zone. Indeed, comparison of the rate of closure over the first 2 min showed that controls closed faster than all of the experimental groups with the exception of the C2 Chim manipulations (Figure 7).

Computational modeling results

To better understand the potential effects of these GTPase signaling manipulations on observed GTPase patterns, we utilized a mathematical model to incorporate and test those potential effects. Our aim was to compare three aspects between model predictions and experimental data: 1) the effect of manipulations on GTPase zone intensities, 2) the effect of manipulations on background GTPase intensities (away from the wound), and 3) the resulting changes in the spatio-temporal aspects of the zones (location, width, and/or overlap). In each case, we sought to compare the results of modest suppression and modest elevation of the GTPases to the control cells.

To do so, we built on a previous mathematical model for Rho-Abr-Cdc42 signaling at single-cell wounds that accounts for the primary features of the time course of spatial patterning (Simon *et al.*, 2013; Holmes *et al.*, 2016). This model (see *Modeling Methods* for details) assumes direct positive feedback between Rho and Abr, a GEF connection from Abr to both Rho and Cdc42, a (more dominant) GAP action of Abr on Cdc42, and positive feedback from Cdc42 to its own activation (Figure 8A), all of which are motivated by previous experimental studies (Chuang *et al.*, 1995; Vaughan *et al.*, 2011). The resulting model consists of three partial differential equations (PDEs) for the spatiotemporal interactions of these three components. These equations include several specific parameters, such as rates of (in)activation, amounts of inactive Rho and Cdc42 that are available to be activated, and feedback parameters. We asked whether the original model, with suitable parameter variations, could also account for our new observations, or, if not, where it fails and how this informs future rounds of models and experiments.

Our first step was to investigate the original model, with relevant model parameters altered to reflect hypothesized effects of the experimental manipulations. We assumed, for example, that low-level

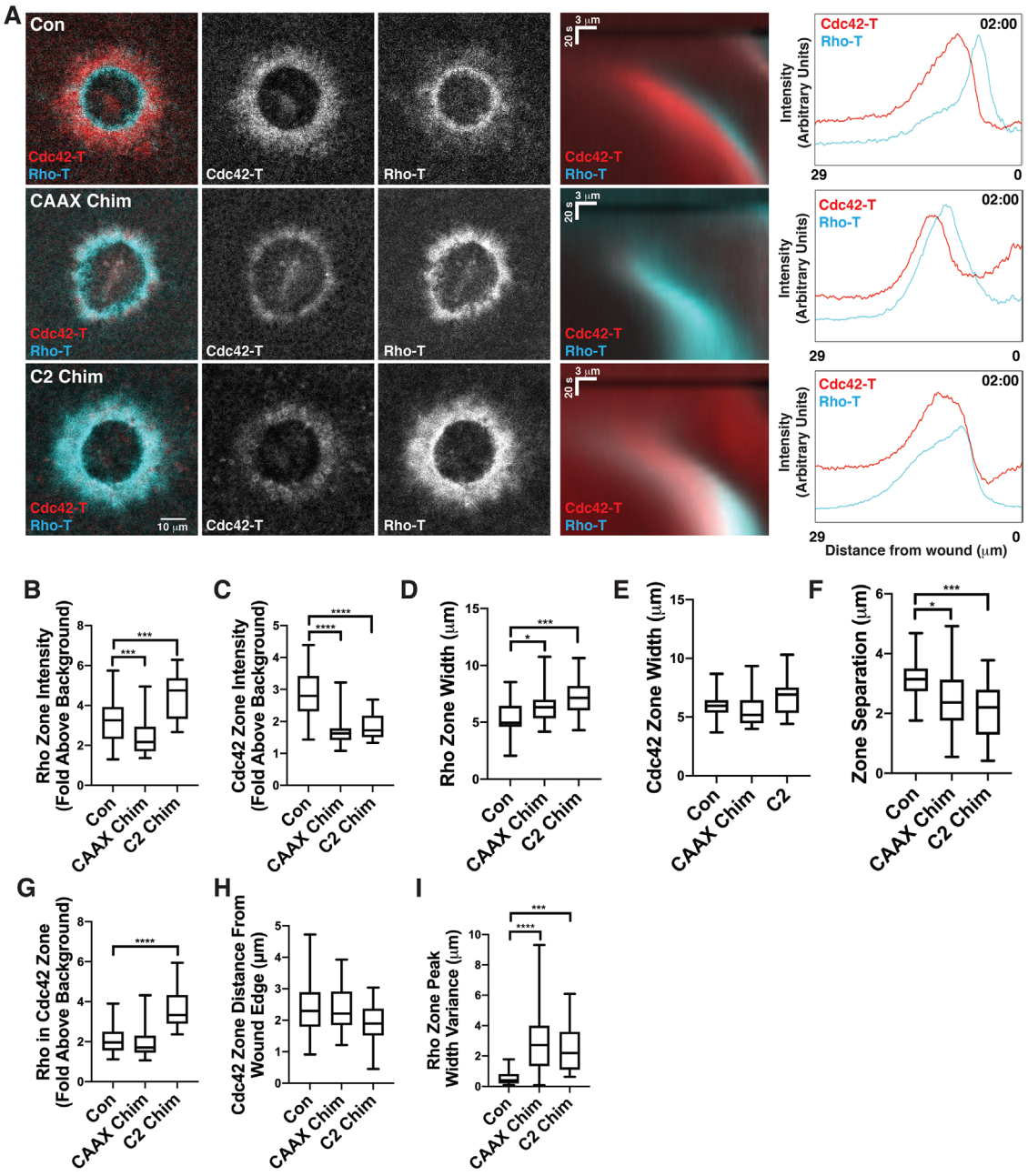

FIGURE 5: Low-level Cdc42 suppression spreads the Rho zone. (A) Left: single frames from 2 min postwounding of controls (Con), cells microinjected with a plasma membrane-targeted Rac and Cdc42 GAP domain (CAAX Chim), or a wound-targeted Rac and Cdc42 GAP domain (C2 Chim) labeled as in Figure 1. Middle: kymographs corresponding to movies from which stills on the right were obtained. Right: line scans corresponding to 2 min point on kymographs in the middle. Note the spreading of Rho zone in both experimental groups. (B, C) Quantification of Rho and Cdc42 zone intensity, respectively, at 2 min postwound for control (Con), cells microinjected with a plasma membrane-targeted Rac and Cdc42 GAP domain (CAAX Chim), or a wound-targeted Rac and Cdc42 GAP domain (C2 Chim). (D, E) Quantification of Rho and Cdc42 zone width, respectively, at 2 min postwound for control (Con), cells microinjected with a plasma membrane-targeted Rac and Cdc42 GAP domain (CAAX Chim), or a wound-targeted Rac and Cdc42 GAP domain (C2 Chim). (F) Quantification of GTPase zone separation at 2 min postwound for control (Con) cells microinjected with a plasma membrane-targeted Rac and Cdc42 GAP domain (CAAX Chim) or a wound-targeted Rac and Cdc42 GAP domain (C2 Chim). (G) Quantification of Rho signal in Cdc42 zone at 2 min postwound for control (Con), cells microinjected with a plasma membrane-targeted Rac and Cdc42 GAP domain (CAAX Chim), or a wound-targeted Rac and Cdc42 GAP domain (C2 Chim). (H) Quantification of Cdc42 zone distance from wound edge at 2 min postwound for control (Con), cells microinjected with a plasma membrane-targeted Rac and Cdc42 GAP domain (CAAX Chim), or a wound-targeted Rac and Cdc42 GAP domain (C2 Chim). (I) Quantification of the Rho zone peak width variance at 2 min postwound for control (Con), cells microinjected with a plasma membrane-targeted Rac and Cdc42 GAP (CAAX Chim), or a wound-targeted Rac and Cdc42 GAP domain (C2 Chim). *$p < 0.05$, **$p < 0.01$, ***$p < 0.005$, ****$p < 0.0001$; (B–H) one-way ANOVA; (I) Brown-Forsythe test. Con $n = 32$ cells; CAAX Chim $n = 28$ cells; C2 Chim $n = 17$ cells.

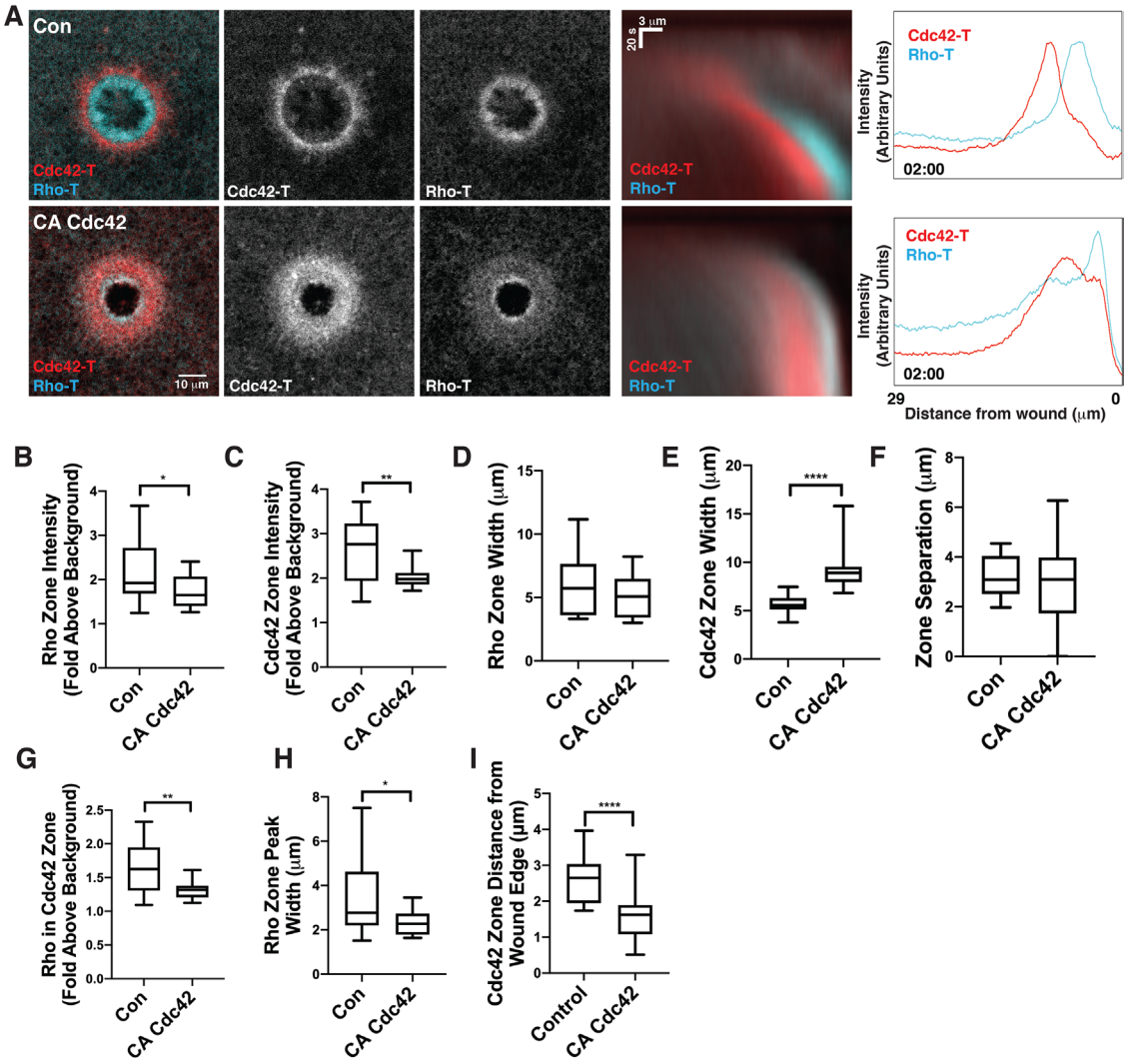

FIGURE 6: Low-level Cdc42 elevation narrows the Rho zone. (A) Left: single frames from 2 min postwounding of controls (Con), or cells microinjected with CA Cdc42 labeled as in Figure 1. Middle: kymographs corresponding to movies from which stills on the right were obtained. Right: line scans corresponding to 2 min point on kymographs in the middle. Note narrowing of Rho zone in CA Cdc42-injected sample. (B, C) Quantification of Rho and Cdc42 zone intensity, respectively, at 2 min postwound for control (Con) or cells microinjected with CA Cdc42. (D, E) Quantification of Rho and Cdc42 zone width, respectively, at 2 min postwound for control (Con), or cells microinjected with CA Cdc42. (F) Quantification of GTPase zone separation at 2 min postwound for control (Con), or cells microinjected with CA Cdc42. (G) Quantification of Rho signal in Cdc42 zone at 2 min postwound for control (Con), or cells microinjected with CA Cdc42. (H) Quantification of Rho zone peak width at 2 min postwound for control (Con), or cells microinjected with CA Cdc42. (I) Quantification of Cdc42 zone distance from wound edge at 2 min postwound for control (Con), or cells microinjected with CA Cdc42. *$p < 0.05$, **$p < 0.01$, ****$p < 0.0001$; one-way ANOVA; Con $n = 12$ cells; CA Cdc42 $n = 15$ cells.

Rho suppression (via DN Rho or C3) reduces the rate of Rho activation (reduced value for a_R). For the manipulations designed to modestly elevate GTPase activity (e.g. CA Rho or CAAX-Larg), we initially considered the hypothesis that persistently active GTPases provide continuous positive feedback to the signaling network (over and above the feedback contribution by endogenous active GTPase). This effect was implemented using additive constants (C_{CA}, R_{CA}) in feedback-activation terms for both Cdc42 and Abr (see *Modeling Methods*).

We utilized two basic methods of analyzing this model and the effects of parameter variations within it. Full spatio-temporal simulations of the model are used to predict the actual spatial dynamics of patterning. However, before applying simulations, we first study how the stable steady states of the system depend on model parameters. This preliminary step helps to determine how manipulations affect zone and background GTPase activity levels, as explained below. For this step, we reduced the full spatially distributed model to one that retains only the kinetic terms (spatially "well-mixed" variant).

Because wounded cells have two distinct GTPase activity levels (a high activity zone near the wound and a low activity state elsewhere), we initially parameterize the model to assure coexistence of such steady states (i.e., conditions for so-called "bistability"). We then examined how steady-state levels associated with the GTPase zone intensities depend on model parameters. Formally, we used bifurcation analysis to do so. This consists of mathematically

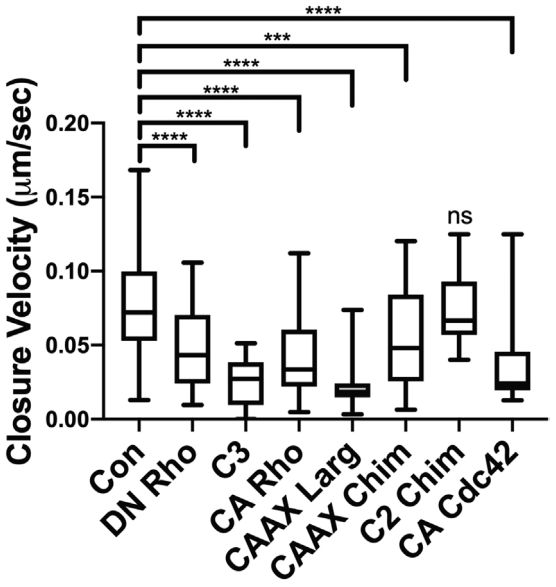

FIGURE 7: Disruption of patterns via low-level GTPase manipulation slows closure of the Cdc42 zone. Comparison of the forward displacement velocity of the Cdc42 zone in the first 2 min postwounding in controls and the various GTPase manipulations employed in this study. ***$p < 0.005$, ****$p < 0.0001$; one-way ANOVA; Con $n = 142$ cells; DN Rho $n = 19$ cells; C3 $n = 21$ cells; CA Rho $n = 23$ cells; CAAX-Larg = 23 cells; CAAX Chim = 28 cells; C2 Chim = 17 cells; CA Cdc42 = 15 cells.

"tuning" (increasing and decreasing) the parameter of interest to assess and plot how the relevant zone and background intensity levels are predicted to change according to the model. The resulting bifurcation diagrams enable us to check whether the model agrees with experimental results on enhancement or suppression of GTPase zone and background intensities.

Each bifurcation diagram (Figure 8, B–E) summarizes the possible range of behaviors as a parameter is varied. Solid curves represent stable steady-state intensities and dashed curves represent unstable steady states of either active Cdc42 (red) or active Rho (blue), while higher curves represent higher zone intensities and lower curves represent background intensities away from the wound. Thus, the curves demonstrate how the WT background and zone intensities change when the perturbation is titrated in the direction indicated by the arrows.

The results show that the original model accounts well for data from experiments with modest suppression in GTPase activity. Recall that we made the assumption that reduced GTPase activity is represented by reduction in the overall Rho activation parameter a_R. Bifurcation analysis results (Figure 8, C and E) illustrate that this assumption is consistent with experimental observations about zone intensities. Specifically, titrating in DN Rho or C3 reduces the Rho zone intensity substantially (as revealed by the steep decline in the upper branch of the blue curve as a_R is reduced) while modestly increasing the Cdc42 zone intensity (as revealed by a shallow increase in the upper red curve in the direction of the arrow). Similarly, titrating in either CAAX Chim or C2 Chim leads to a substantial reduction in Cdc42 zone intensity while leaving the Rho zone intensity unaffected. These model predictions support the hypothesis that DN perturbations lead to a drop in the GTPase activation rates.

It would be natural to assume, analogously, that a modest elevation of GTPase would lead to an increase in overall activation rates (a_R, or a_C). However, model results associated with the manipulations designed to modestly elevate GTPase activity are inconsistent with experimental observations. That is, the model predicts that CA Rho should *increase* Rho zone intensity modestly (with a small decrease in Cdc42 intensity; Figure 8D). This is clearly not the case according to Figure 3, where we found that CA Rho results in a substantial reduction in Rho zone intensity. Similarly, while the model predicts that CA Cdc42 should *increase* Cdc42 zone intensity modestly (without affecting Rho zone intensity; Figure 8B), experimental results (Figure 6) show the opposite, a reduction in Cdc42 intensity, although as noted above, this conclusion is complicated by the impact of CA Cdc42 on Cdc42 background levels. We can also reject the idea that such experimental data can be represented by reduced GTPase inactivation rates, since the bifurcation plots are essentially identical to those for increased a_R (a decrease in a deactivation rate has an effect that is similar to an increase in the activation rate; results not shown).

We thus next asked whether CA Cdc42 or Rho might simply enhance the extent of positive feedback, for example, by continual signaling to unidentified GEFs (Figure 8A, middle). The essential idea here is that a CA protein residing on the membrane may participate in the same feedback as the wild-type protein, but not be subject to membrane cycling or inactivation. Consequently, we investigated a model variant with nonzero values of C_{CA} and R_{CA} (Figure 8, B and D). We found that, as before, resulting bifurcation plots were inconsistent with experimental data. That is, an increase in C_{CA} (resp. R_{CA}) is predicted to increase the Cdc42 (resp. Rho) zone intensity, whereas observations show the opposite trend, reduced zone intensities.

In view of the inconsistency in the predictions for the manipulations designed to modestly elevate GTPase activity, we revised our hypothesis. Specifically, we tested the possibility that CA Rho leads to a reduction in Abr signaling that lies at the hub of this signaling network (Figure 8A, bottom). This idea is motivated by the observation that CA Rho leads to a reduction in Rho intensity, a reduction in Cdc42 intensity (Figure 3), as well as a redistribution of Abr (Figure 4). For the moment, we can only speculate as to why this might occur. One possibility is that the addition of CA Rho globally absorbs Abr, affecting its availability. This is plausible, as prior results indicate that high levels of CA Rho globally recruit Abr (Vaughan *et al.*, 2011). However, the modest levels of CA Rho applied here do not lead to a significant elevation in background Abr (Figure 4), and so this remains a speculative possibility. An alternative potential explanation is that a local limitation of Abr at the wound site, in conjunction with CA Rho application, could lead to a broadening of the Abr zone, spreading a limited amount more widely and hence reducing its intensity. This redistribution of Abr (broader zone with reduced intensity) is observed experimentally (Figure 4). This possibility, however, raises the question of what could account for limited local Abr availability at the wound. As the wound size is small relative to the cell size, one would ab initio expect availability of cytosolic Abr to be essentially unlimited. Membrane localization or some other unknown mechanism may account for such hypothesized Abr limitation.

For CA Cdc42, we considered the possibility that it binds and occupies the GEF/GAPs that normally facilitate GTPase cycling on and off the membrane. We account for this by assuming that the global pool of cytosolically available inactive Cdc42, C_i, is reduced due to impaired recycling.

The revised hypotheses for the mechanisms underlying CA Rho and CA Cdc42 are more closely consistent with data. Bifurcation diagrams (Figure 8, B and D) illustrate how varying inactive protein

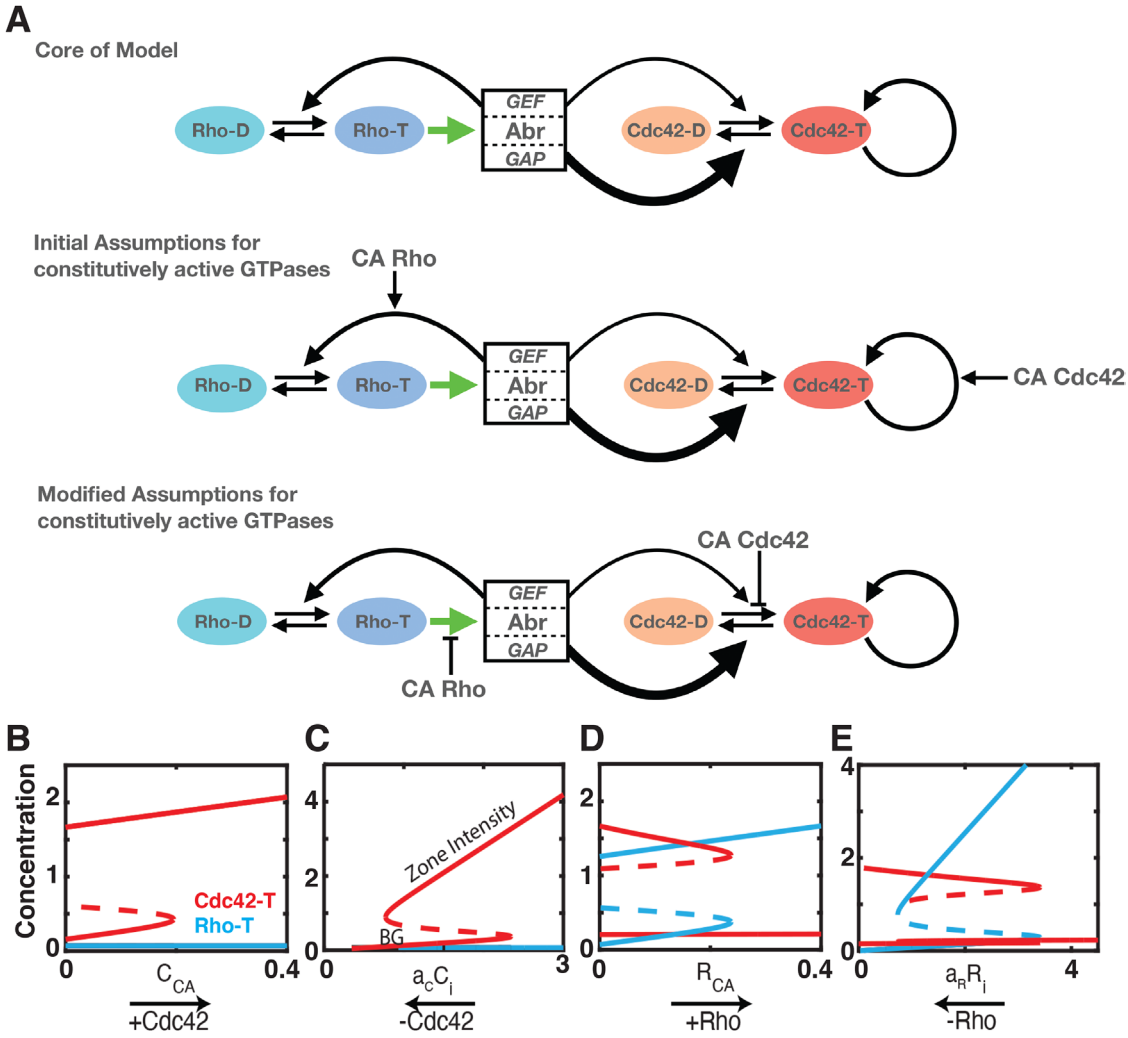

FIGURE 8: The nonspatial, well-mixed model captures the effects of low-level GTPase reduction but not low-level GTPase activation. (A) Top: a schematic diagram showing the basic player interactions assumed by the computational model. Abr activates Rho and Cdc42 via its GEF domain while inactivating Cdc42 via its GAP domain. Active Rho promotes Abr activity. Middle: initially, model assumes that CA Rho and Cdc42 enhance positive feedback. Bottom: subsequently, model assumes that CA Rho and Cdc42 reduce availability of GEFs. (B–E) Bifurcation plots of the reduced ("well-mixed," nonspatial variant) model with respect to parameters representing hypothesized effects of modest increases (+) and decreases (-) of GTPase activity. The horizontal axis label indicates the parameter that is varied and the corresponding experimental treatment being described. (B) The effect predicted by the model of CA Cdc42 concentration (C_{CA}) on zone and background intensities. (C) The predicted effect of scaling up the rate of Cdc42 activation or changing the availability of inactive Cdc42 ($a_C\ C_i$). (D) The effect of CA Rho (R_{CA}). (E) The effect of scaling up the rate of Rho activation or changing the availability of inactive Rho ($a_R\ R_i$). The + and – signs associated with the arrows indicate the directions associated with elevating and suppressing GTPase activity, respectively (for example, –Cdc42 suppression decreases a_C). Solid (dashed) lines represent stable (unstable) activity states. Over a range of parameter values, the high activity around the wound ("zone intensity," upper solid curves) coexists with the background activity level (lower solid curves, "BG"). Dashed curves (unstable steady states) represent thresholds separating the background and high activity steady states. Red = active Cdc42 (Cdc42-T); blue = active Rho (Rho-T). See text for details.

concentrations will lead to the same intensity changes observed experimentally. Note that "activation rates" and "concentrations of inactive GTPases" have the same effect in the model. Thus, the same bifurcation diagrams illustrate both changes in activation (explored above with regard to the suppressed GTPase conditions) and GTPase available for activation (explored here with respect to the elevated GTPase conditions).

We asked how these updated hypotheses for the effects of the elevated proteins (and original hypotheses for reduced protein treatments) play out over space adjoining the wound. Here we use standard numerical techniques for solving reaction-diffusion equations (details in *Modeling Methods*) with initial stimuli of Rho and Cdc42 close to the "wound" and no flux of proteins at the boundaries of the one-dimensional (1D) domain. The transient result is plotted as a set of spatial active GTPase profiles in 1D, representing distance away from the wound. Figure 9 shows snapshots of the GTPase and Abr spatial distributions for both kinds of conditions. For the elevated Rho treatment, the model predicts a reduction in Rho zone intensity, consistent with experimental observations. Model predictions for the elevated Cdc42 with the revised hypothesis are also

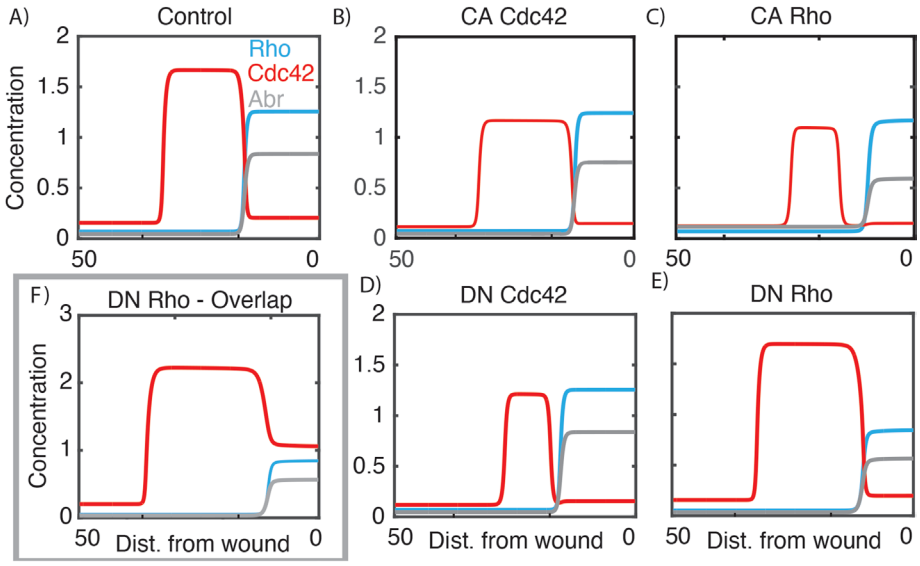

FIGURE 9: Spatial model simulations capture some of the effects of low-level GTPase elevation. Model results showing the relative positions and intensities of active Rho (blue), Cdc42 (red), and Abr (gray). Wound is on the right. Results from simulations of control (Con), as well as results obtained with parameters altered to represent the effects of CA Cdc42, CA Rho, DN Cdc42, and DN Rho are shown. See text for details.

consistent with the reduction in Cdc42 zone intensity (Figure 9, CA Cdc42).

Overall, our model supports the following mechanisms. 1) Perturbations that suppress the level of GTPases lead to reduced rates of activation of the GTPases. 2) Perturbations that globally elevate the GTPases have the less intuitive effect of attenuating signaling by either globally or locally limiting GTPase and Abr availability on wounding. While the enhanced level of proteins may participate in the same signaling feedbacks as the WT forms, that, on its own, did not suffice to explain our observations in the context of the existing WT model.

So far, we have described model variants that account only for observed zone intensities. There are, however, two particularly salient observations regarding the zone localizations: low-level suppression of Rho activity results in merging of the Rho and Cdc42 zones, while low-level elevation of Rho activity results in greater separation of the Rho and Cdc42 zones. With the updated assumptions about the effects of CA Rho, the model illustrates the same zone separation (Figure 9, CA Rho), in agreement with data. Initial DN Rho simulations do not give rise to the same zone overlap observed experimentally (Figure 9, DN Rho). However, we hypothesized that this overlap is a result of the impaired Rho zone intensity being insufficient to suppress Cdc42 via Abr. To test this, we directly manipulated the threshold at which Abr suppresses Cdc42 activity by altering the Cdc42 inactivation rate parameters. By reducing the d_C parameter from 0.8 to 0.6, we find that the Rho zone is subsumed by the Cdc42 zone in the Rho suppression condition while still maintaining Cdc42 exclusion in the control case (Figure 9, DN Rho-Overlap). Agreement with experiments is not perfect, however; the model predicts that at the overlap, Cdc42 intensity should be reduced (though still elevated above background). This contrasts with experimental findings. However, the modeling does support the hypothesis that, in the Rho suppression condition, Rho intensity is sufficiently reduced that it cannot exclude Cdc42. However, it is still unclear why the remaining Rho does not appear to impact Cdc42 at all.

With respect to the consequences of low-level Cdc42 suppression, modeling efforts were frustrated by the variability of the results. In particular, CAAX Chim lowered Rho zone intensity, C2 Chim elevated Rho zone intensity, and DN Cdc42 produced a spectrum of inconsistent results, making it impossible to generate a model that reproduces the observed effects (Figure 9, DN Cdc42). Potential reasons for this are discussed below.

DISCUSSION

The first finding of this study is that the level of Rho activity determines the placement of the Cdc42 zone relative to the Rho zone and the wound edge. That is, experimental reduction of the intensity of the Rho zone results in displacement of the Cdc42 zone such that it becomes positioned at the wound edge and completely overlaps the Rho zone. The current modeling results as well as previous work showing that the dual GEF-GAP Abr is recruited to the Rho zone via active Rho (Vaughan *et al.*, 2011), where it serves to limit Cdc42 activity, could explain this finding: once Rho activity drops below threshold, insufficient Abr is recruited to keep the Cdc42 at bay. As a result, the Cdc42 is no longer excluded from the Rho zone and is free to concentrate at the wound edge. Consistent with this modeling result, previous work demonstrated that suppression of Rho activation resulted in reduction of Abr recruitment to wounds (Vaughan *et al.*, 2011).

These results are complemented by the demonstration that two different manipulations designed to modestly elevate Rho activity—CA Rho and CAAX-Larg—have the opposite effect as Rho reduction, namely, increased separation of the Rho and Cdc42 zones and an increase in the distance of the Cdc42 zone from the wound edge. Here again the modeling findings suggest that the key player is Abr, but the mechanism involved is even less intuitive than that leading to the zone merging. That is, the increased separation could be explained by a global increase in cortical Abr recruitment at the expense of the Abr available for the Rho zone. Thus, the Rho zone is in effect partially starved for Abr, while the Cdc42 zone is displaced from the wound edge as a result of more Abr-dependent Cdc42 inactivation. Consistent with this proposition, direct analysis of Abr demonstrated that CA Rho expression both broadens and dilutes the Abr zone.

The second finding of this study is that where the outer edge of the Rho zone forms is critically dependent on the level of Cdc42 activity. That is, experimental reduction of the intensity of the Cdc42 zone results in broadening of the Rho zone activity peak, while experimental expansion of the Cdc42 zone results in narrowing of the Rho zone peak. Because it was previously shown that the rate of Rho inactivation is sharply elevated where it overlaps with the leading edge of the Cdc42 zone (Burkel *et al.*, 2012), this result could be explained if active Cdc42 recruits GAPs or other players that promote Rho inactivation (not modeled in the current paper). The observation of the Rho "plateau" described here is consistent with this hypothesis. However, there are two problems with this hypothesis. First, in some control samples, the plateau appears to begin ahead of (toward the wound) the peak of Cdc42 activity (see Figure 1).

Second, if the Cdc42 zone simply defines the outer boundary of the Rho zone via local Rho inactivation, it would be predicted that complete loss of the Cdc42 zone would both broaden and brighten the Rho zone. Instead, complete loss of the Cdc42 zone is accompanied by complete loss of the Rho zone (Supplemental Figure S5; see also Benink and Bement, 2005).

Presumably, more information about the means by which Rho is inactivated at the trailing edge of its zone and the development of a new round of modeling will help to resolve these discrepancies.

Computational modeling suggests that the effects of modest reductions in Cdc42 and Rho on zone intensity could be explained by the resulting reduction in GTPase activity. However, it appears that the explanation for the effects of their modest elevations is more complex. The natural assumptions that the added Cdc42/Rho forms participate in the same feedbacks as the existing GTPases predict that their presence would intensify zone activities, which is in fact completely opposite of what is observed experimentally. Instead, modeling results suggest that the global elevation in GTPase activity in these manipulations may be restricting available GTPase effectors such as Abr and other GEFs or GAPs. While this restriction is sufficient to explain the observations here, the underlying mechanism requires further study.

Computational results also provide hints as to why Rho manipulations alter the localization of the Cdc42 zone. That is, the modeling results suggest that when modest reductions in Rho activity are applied, that reduction appears to attenuate Abr signaling sufficiently that it no longer strongly inhibits Cdc42 near the wound. On the other hand, the global Abr restriction resulting from modest Rho elevation needed to explain the Rho zone attenuation in that case also leads to the separation of Rho and Cdc42 zones observed experimentally. The model, in its current form, does not explain how Cdc42 activity determines the location of the Rho zone's outer border. In the model's current form, Rho and Abr activity are completely unaffected by Cdc42. Thus, additional future modeling along with new data will be required to assess whether Cdc42 is directly affecting Rho signaling or is doing so through some other indirect means such as competing for shared molecules.

The above findings are specific to cell repair, but the results of this study could also be of importance for more general conclusions about GTPase patterning. In particular, it is striking that the constitutively active Rho and Cdc42 mutants reduce the intensity of their target zones, as does the CAAX-Larg construct. While both experiment and modeling potentially explain the effects of the CA Rho and CAAX-Larg as resulting from global recruitment of Abr, this mechanism does not explain the effects of CA Cdc42, since expression of this mutant does not result in global cortical recruitment of Abr (Vaughan *et al.*, 2011). Because CA Cdc42 broadens the Cdc42 zone while potentially reducing its intensity, we suspect that this manipulation acts by reducing GTPase flux (Bement *et al.*, 2006), just as CA Rho is thought to do during cytokinesis (Miller and Bement, 2009; Yoshida *et al.*, 2009).

The demonstration that even modest changes in Rho and Cdc42 activity can have profound effects on GTPase patterning and the speed of zone closure is important not only for cell repair but may also be important for other situations in which the GTPases are deployed in distinct cortical patterns. For example, it would be of considerable interest to assess the effects of low-level GTPase manipulation on other processes that entail GTPase pattern formation such as cell locomotion (Pertz *et al.*, 2008; Machacek *et al.*, 2009), or formation of cell–cell junctions (Priya *et al.*, 2013; 2015; Reyes *et al.*, 2014; Breznau *et al.*, 2015).

Finally, we note that the use of the C2 domain of PKCβ to target exogenous constructs described here could be useful in any situation where calcium elevation near the plasma membrane occurs. The potential for promoting cell repair is obvious: by fusing C2 with positive regulators of the repair response (e.g., calpains [Mellgrem *et al.*, 2007; Piper *et al.*, 2020] or MG53 [Cai *et al.*, 2009]), it may be possible to up-regulate healing in cells with repair deficits without the danger of constitutive recruitment. Similarly, in other situations where cells experience transient increases in plasma membrane-proximal calcium (e.g., spines and synapses in neurons), C2 domain fusions could allow reversible and specific recruitment of different proteins. Significantly, expression of C2-Chim was the only Cdc42 manipulation that did not result in alteration of prewound background levels of Rho and Cdc42 activity. This not only supports the usefulness of C2 fusions for time-resolved manipulation of the wound response but also provides a potential explanation for the maddening variability resulting from the other Cdc42 manipulations: in contrast to C2-Chim, DN Cdc42, CAAX-Chim, and CA Cdc42 almost certainly alter the cortical cytoskeleton prior to wounding based on their effect on prewound Cdc42 activity. Thus, their effects likely represent a combination of their impact on the Cdc42 zone as well the cortical cytoskeleton prior to wounding.

MATERIALS AND METHODS

Request a protocol through *Bio-protocol*.

Oocyte acquisition and preparation

Ovarian tissue was obtained from adult *Xenopus laevis* females via surgical procedures approved by the University of Wisconsin–Madison Institutional Animal Care and Use Committee. Tissue was maintained at 16°C in 1× -modified Barth's solution (88 mM NaCl, 1 mM KCl, 2.4 mM $NaHCO_3$, 0.82 mM $MgSO_4$, 0.33 mM $NaNO_3$, 0.41 mM $CaCl_2$, and 10 mM 4-[2-hydroxyethyl]-1-piperazineethanesulfonic acid [HEPES], pH 7.4, supplemented with 100 µg/ml gentamicin sulfate, 6 µg/ml tetracycline, and 25 µg/ml ampicillin). Follicle cell sheaths were removed from oocytes by incubation in 1× Barth's solution containing 8 mg/ml type I collagenase (Life Technologies, Grand Island, NY) at 16°C on a 60-rpm rotating plate followed by extensive rinsing in 1× Barth's solution and manual dissociation. Defolliculated oocytes were stored in 1× Barth's solution at 16°C until use.

Construct generation, mRNA preparation and oocyte microinjection

DN (N19), CA (V14) *Xenopus* Rho and DN (N17) and CA (V12) *Xenopus* Cdc42 in PCS2 were generated using a modified version of the Quickchange protocol (Agilent). For the CAAX and C2-targeted constructs, versions of pCS2 were made with a flexible linker (SAGGX5) followed by either a CAAX box (Reyes *et al.*, 2014) or the C2 domain of protein kinase Cβ (Davenport *et al.*, 2016). CAAX-Larg was generated by cloning the catalytic domain of Human Larg (AA 766-997; a gift from Michael Glotzer, University of Chicago) upstream of SAGGX5 in the CAAX pCS2; CAAX-Chim was generated by cloning the catalytic domain of *Xenopus* Chimaerin 1 (AA 258–459) upstream of SAGGX5 in the CAAX pCS2, and C2 Chim was generated by cloning the catalytic domain of *Xenopus* Chimaerin 1 upstream of SAGGX5 in the C2 pCS2.

mRNAs were transcribed using mMessage mMachine SP6 Transcription Kit (Life Technologies) and purified using RNeasy Mini Kit (Qiagen, Hilden, Germany). Transcript size was verified on 1% agarose/formaldehyde denaturing gels versus Millennium Marker (Life Technologies) molecular weight standard. Oocytes were injected

while in 1× Barth's solution with a 40-nl injection volume. mRNAs were injected at the following needle concentrations: mCherry-wGBD at 166 ng/µl, 3XGFP-rGBD at 100 ng/µl, DN Rho at 80 ng/µl, CA Rho at 20 ng/µl, CAAX-Larg at 1 ng/µl, DN Cdc42 at 62.5 ng/µl, CAAX Chim at 10 ng/µl, and C2 Chim at 125 ng/µl. C3 was injected at a needle concentration of 0.05 ng/µl. mRNAs were injected 20–24 h before wounding; C3 was injected 1 h before wounding. To achieve low-level activation or suppression of Rho GTPases, DN and CA mutant GTPase constructs were allowed to express half as long as in previous work (Benink and Bement, 2005). Oocytes were allowed to recover for 30–60 min after each microinjection and maintained at 16° until the start of the experiment. Following overnight expression, the distribution of oocyte pigment was used as a qualitative assay of cell health: oocytes with obvious disruptions in the normal pattern of pigment distribution were considered unhealthy and not used for experiments. Titering of mRNA expression (see *Results*) was based on two criteria: the extent to which GTPase activity background was elevated prior to wounding and whether discernable GTPase zones formed. For the reasons described in the *Results*, concentrations or times of mRNA expression that resulted in overt elevation of GTPase activity prior to wounding, or which completely suppressed zone formation, were considered unacceptable; concentrations and times of expression that had no overt effect on prewound GTPase activity and which permitted the formation of both zones, but which nevertheless produced wound phenotypes, were considered acceptable. The exception to this was CA-Cdc42, for which we were unable to obtain a concentration or time of expression regime that reliably produced a phenotype without altering prewound GTPase activity (see *Results*).

Image acquisition, wounding, and data analysis

Samples were imaged on a Nikon Eclipse Ti inverted laser-scanning confocal microscope equipped with a Prairie Point Scanner (Bruker, Middleton WI) with a 60×, 1.4 NA oil objective. Cells were wounded with a 440-nm dye laser pumped by a MicroPoint 337-nm nitrogen laser (Andor, South Windsor, CT). The wounding laser is nominally diffraction limited and manually activated for ~1 s with a ~5- to 10-Hz repetition rate, and the source laser (per manufacturer specifications) has a maximal output of 400 µJ/pulse. Wounded cells were imaged using six 1-µm optical sections. Imaging data were processed using Fiji (Schindelin *et al.*, 2012). To generate radially averaged kymographs, projected tif stacks were radially averaged after manually selecting the center of the wound using the radial reslice function in the Fiji stacks menu. Radially resliced samples were converted to average intensity projections to generate kymographs. All line scan movies and stills were generated from kymographs in two steps as laid out in Supplemental Figure S1: first, they were resliced into 1-px wide strips and converted to a tif stack using RollingSelection, an in-house plugin. Then the stack was converted to a movie using Plot Profile followed by the LiveGraphToStack plugin. Background levels, zone intensities, and relative amounts of zone pollution (i.e., the amount of Cdc42 activity within the Rho zone and vice versa) were measured from the radially averaged kymographs; zone widths (at half peak height) and peak zone widths (at 75% peak height) were measured from line scan plots; note that the line scan plots, while useful for visualizing zone features such as width and relative position, should not be used to judge absolute intensities between the different GTPases. Zone separation was measured by drawing a line between the peaks of each zone on line scan plots. The only feature that did not show up well in radially averaged kymographs or line scans was the distance of the Cdc42 zone from the wound edge; this was measured at eight positions around each wound edge in Fiji by drawing a line from the inner (woundward) edge of the Cdc42 zone to the wound edge using grayscale images of Cdc42 activity. Prism8 was used for calculating means, standard deviations, and for statistical measurements. All experimental quantifications are based on a minimum of at least 14 cells from at least two independent experiments (i.e., oocytes obtained from different frogs).

MODELING METHODS

The wound has radial symmetry. We simplify the geometry by simulating the equations in one spatial dimension (1D), with x representing distance from the wound edge. The variables $R(x,t)$, $C(x,t)$, $A(x,t)$ denote concentrations of active, membrane-bound Rho, Cdc42, and Abr. Inactive forms of Rho (R_i) and Cdc42 (C_i) are assumed to be spatially uniform, but possibly affected by the GTPase manipulations.

The reaction-diffusion equations for our model are then as follows:

$$\frac{\partial R}{\partial t} = a_R\left(b_R + \gamma_R \frac{A^6}{K_R^6 + A^6}\right)R_i - dR + D\Delta R$$

$$\frac{\partial C}{\partial t} = a_C\left(b_C + \gamma_{AC}\cdot A + \gamma_C \frac{(C+C_{CA})^6}{K_C^6 + (C+C_{CA})^6}\right)C_i - (d_C + d_{AC}\cdot A)C + D\Delta C$$

$$\frac{\partial A}{\partial t} = \gamma_{RA}(R + R_{CA}) - d_A A + D\Delta A$$

In each equation, the terms in first round braces are rates of activation, the negative terms are rates of inactivation and the terms with coefficients D represent diffusion. Here, parameters labeled (a) indicate scaling parameters that control the general rates of activation, (b) indicate basal activation rates, (d) indicate deactivation rates, (γ) indicate feedback strength parameters, (K) are Hill function thresholds, and (C_i and R_i) represent the concentration of the pool of available inactive GTPases (assumed constant). Detailed meanings and values of all parameters are given in Table 1. The powers $n = 6$ in the Hill functions are the same as in the original model from (Simon *et al.*, 2013). Any value $n > 3$ suffices to obtain similar results, though larger values yield more substantial regions of bistability in the parameter space. (C_{CA} and R_{CA}) account for the presence of CA proteins that participate in activation feedbacks but do not undergo cyclical (in)activation themselves. A 50-µm 1D domain is used for simulation purposes and all species are assigned a diffusion rate of 0.1 µm^2/s. This rate of diffusion matches the observed order of magnitude of diffusion for membrane bound GTPases. All kinetic parameters (see Table 1) were chosen in ranges consistent with bistability to represent coexistence of the background and zone intensities. Neumann (no-flux) boundary conditions are assumed for R, C, and A at the ends of the 1D domain. A small initial zone of active Rho and active Cdc42 is taken for initial conditions to set off the patterning. Simulation snapshots are plotted at time T = 40, which suffices for GTPase zones to form their full activation levels. In its present form, the model does not include a mechanism to halt the spread of Cdc42 activity, though including a limited pool of recruitable Cdc42 easily fixes this spread.

For the bifurcation analysis, the spatial diffusion terms were dropped, and the resulting ordinary differential equations for R, C, and A were considered. All bifurcation analyses in this article were performed using Matcont, a MATLAB-based numerical continuation package for ODE systems. All spatial simulations were performed using a custom PDE solver using a Crank Nicolson treatment of the

Parameter	Base value (condition = value)	Meaning
γ_{RA}	1 (CA Rho = 0.65)	Feedback (Rac→Abr activation)
d_A	1.5	Basal Abr deactivation rate
a_C	0.1	Cdc42 activation rate scaling
b_C	1	Basal Cdc42 activation rate
γ_{AC}	3	Rate Abr activates Cdc42
γ_C	11	Feedback (Cdc42→ Cdc42 activation)
K_C	0.7	Cdc42 Hill threshold
d_C	0.8 (DN Rho Fig 9f = 0.6)	Basal Cdc42 deactivation rate
d_{AC}	1.5	Abr→ Cdc42 deactivation rate
C_i	1.2 (DN Cdc42 = 0.9, CA Rho = 0.92)	Inactive Cdc42 conc.
C_{CA}	0 (CA Cdc42 = 0.13)	CA Cdc42 conc.
a_R	0.07	Rac activation rate scaling
b_R	1	Basal Rac activation rate
γ_R	17.1	Feedback (Abr→Rac activation)
K_R	0.4	Abr Hill threshold
R_i	1 (DN Rho = 0.74)	Inactive Rac Conc.
d_R	1	Basal Rac deactivation rate
R_{CA}	0 (CA Rho = 0.2)	CA Rho conc.
D	0.1	Diffusion rates

TABLE 1: Parameters used in the computational model.

diffusion component of the PDEs and forward Euler treatment of the chemical kinetics. The discrete spatial and temporal step sizes used were $\Delta x = 0.25$ μm and $\Delta t = 0.01$ time units, respectively. Alternative numerical schemes (e.g., Method of Lines) and discretization sizes yield the same patterning results.

ACKNOWLEDGMENTS

This work was supported by an award from the National Institutes of Health to W.M.B. (RO1GM052932), an award from the National Science Foundation to W.H. (NSFDMS1562078), and a Discovery Grant from the Natural Science & Engineering Research Council to L.E.K. We are grateful to our labmates for feedback on this project. Special thanks to Kevin Sonnemann for persistent and vigorous schooling on statistical tests.

REFERENCES

Abreu-Blanco MT, Verboon JM, Parkhurst SM (2011). Cell wound repair in Drosophila occurs through three distinct phases of membrane and cytoskeletal remodeling. J Cell Biol 193, 455–464.

Abreu-Blanco MT, Verboon JM, Parkhurst SM (2014). Coordination of Rho family GTPase activities to orchestrate cytoskeleton responses during cell wound repair. Curr Biol 24, 144–155.

Ahmed S, Lee J, Wen LP, Zhao Z, Ho J, Best A, Kozma R, Lim L (1994). Breakpoint cluster region gene product-related domain of n-chimaerin. Discrimination between Rac-binding and GTPase-activating residues by mutational analysis. J Biol Chem 269, 17642–17648.

Arnold TR, Stephenson RE, Miller AL (2017). Rho GTPases and actomyosin: Partners in regulating epithelial cell-cell junction structure and function. Exp Cell Res 358, 20–30.

Bement WM, Benink HA, von Dassow G (2005). A microtubule-dependent zone of active RhoA during cleavage plane specification. J Cell Biol 170, 91–101.

Bement WM, Mandato CA, Kirsch MN (1999). Wound-induced assembly and closure of an actomyosin purse string in Xenopus oocytes. Curr Biol 9, 579–587.

Bement WM, Miller AL, von Dassow G (2006). Rho GTPase activity zones and transient contractile arrays. Bioessays 28, 983–993.

Bement WM, von Dassow G (2014). Single cell pattern formation and transient cytoskeletal arrays. Curr Opin Cell Biol 26, 51–59.

Benink HA, Bement WM (2005). Concentric zones of active RhoA and Cdc42 around single cell wounds. J Cell Biol 168, 429–439.

Braun U, Habermann B, Just I, Aktories K, Vandekerckhove J (1989). Purification of the 22 kDa protein substrate of botulinum ADP-ribosyltransferase C3 from porcine brain cytosol and its characterization as a GTP-binding protein highly homologous to the rho gene product. FEBS Lett 243, 70–76.

Breznau EB, Semack AC, Higashi T, Miller AL (2015). MgcRacGAP restricts active RhoA at the cytokinetic furrow and both RhoA and Rac1 at cell-cell junctions in epithelial cells. Mol Biol Cell 26, 2439–2455.

Burkel BM, Benink HA, Vaughan EM, von Dassow G, Bement WM (2012). A Rho GTPase signal treadmill backs a contractile array. Dev Cell 23, 384–396.

Cai C, Masumiya H, Weisleder N, Matsuda N, Nishi M, Hwang M, Ko J-K, Lin P, Thornton A, Zhao X, *et al*. (2009). MG53 nucleates assembly of cell membrane repair machinery. Nat Cell Biol 11, 56–64.

Chuang TH, Xu X, Kaartinen V, Heisterkamp N, Groffen J, Bokoch GM (1995). Abr and Bcr are multifunctional regulators of the Rho GTP-binding family. Proc Natl Acad Sci USA 92, 10282–10286.

Citi S, Guerrera D, Spadaro D, Shah J (2014). Epithelial junctions and Rho family GTPases: the zonular signalosome. Small GTPases 5, 1–15.

Clark AG, Miller AL, Vaughan E, Yu H-YE, Penkert R, Bement WM (2009). Integration of single and multicellular wound responses. Curr Biol 19, 1389–1395.

Davenport NR, Bement WM (2016). Cell repair: Revisiting the patch hypothesis. Commun Integr Biol 9, e1253643.

Davenport NR, Sonnemann KJ, Eliceiri KW, Bement WM (2016). Membrane dynamics during cellular wound repair. Mol Biol Cell 27, 2272–2285.

DeKraker C, Goldin-Blais L, Boucher E, Mandato CA (2019). Dynamics of actin polymerisation during the mammalian single-cell wound healing response. BMC Res Notes 12, 420.

Demonbreun AR, Quattrocelli M, Barefield DY, Allen MV, Swanson KE, McNally EM (2016). An actin-dependent annexin complex mediates plasma membrane repair in muscle. J Cell Biol 213, 705–718.

Fritz RD, Pertz O (2016). The dynamics of spatio-temporal Rho GTPase signaling: formation of signaling patterns. F1000Res 5. https://doi.org/10.12688/f1000research.7370.1

Godin LM, Vergen J, Prakash YS, Pagano RE, Hubmayr RD (2011). Spatio-temporal dynamics of actin remodeling and endomembrane trafficking

in alveolar epithelial type I cell wound healing. Am J Physiol Lung Cell Mol Physiol 300, L615–L623.
Golding AE, Visco I, Bieling P, Bement WM (2019). Extraction of active RhoGTPases by RhoGDI regulates spatiotemporal patterning of RhoGTPases. Elife 8. https://doi.org/10.7554/eLife.50471
Goryachev AB, Leda M (2017). Many roads to symmetry breaking: molecular mechanisms and theoretical models of yeast cell polarity. Mol Biol Cell 28, 370–380.
Holmes WR, Golding AE, Bement WM, Edelstein-Keshet L (2016). A mathematical model of GTPase pattern formation during single-cell wound repair. Interface Focus 6, 20160032.
Horn A, Van der Meulen JH, Defour A, Hogarth M, Sreetama SC, Reed A, Scheffer L, Chandel NS, Jaiswal JK (2017). Mitochondrial redox signaling enables repair of injured skeletal muscle cells. Sci Signal 10. https://doi.org/10.1126/scisignal.aaj1978
Kono K, Saeki Y, Yoshida S, Tanaka K, Pellman D (2012). Proteasomal degradation resolves competition between cell polarization and cellular wound healing. Cell 150, 151–164.
Lek A, Evesson FJ, Lemckert FA, Redpath GMI, Lueders A-K, Turnbull L, Whitchurch CB, North KN, Cooper ST (2013). Calpains, cleaved mini-dysferlinC72, and L-type channels underpin calcium-dependent muscle membrane repair. J Neurosci 33, 5085–5094.
Luo JH, Weinstein IB (1993). Calcium-dependent activation of protein kinase C. The role of the C2 domain in divalent cation selectivity. J Biol Chem 268, 23580–23584.
Machacek M, Hodgson L, Welch C, Elliott H, Pertz O, Nalbant P, Abell A, Johnson GL, Hahn KM, Danuser G (2009). Coordination of Rho GTPase activities during cell protrusion. Nature 461, 99–103.
Mandato CA, Bement WM (2001). Contraction and polymerization cooperate to assemble and close actomyosin rings around Xenopus oocyte wounds. J Cell Biol 154, 785–797.
Martin K, Reimann A, Fritz RD, Ryu H, Jeon NL, Pertz O (2016). Spatio-temporal co-ordination of RhoA, Rac1 and Cdc42 activation during prototypical edge protrusion and retraction dynamics. Sci Rep 6, 21901.
Mellgren RL, Zhang W, Miyake K, McNeil PL (2007). Calpain is required for the rapid, calcium-dependent repair of wounded plasma membrane. J Biol Chem 282, 2567–2575.
Miller AL, Bement WM (2009). Regulation of cytokinesis by Rho GTPase flux. Nat Cell Biol 11, 71–77.
Miyake K, McNeil PL, Suzuki K, Tsunoda R, Sugai N (2001). An actin barrier to resealing. J Cell Sci 114, 3487–3494.
Moe AM, Golding AE, Bement WM (2015). Cell healing: Calcium, repair and regeneration. Semin Cell Dev Biol 45, 18–23.
Nakamura M, Dominguez ANM, Decker JR, Hull AJ, Verboon JM, Parkhurst SM (2018). Into the breach: how cells cope with wounds. Open Biol 8. https://doi.org/10.1098/rsob.180135
Nakamura M, Verboon JM, Parkhurst SM (2017). Prepatterning by RhoGEFs governs Rho GTPase spatiotemporal dynamics during wound repair. J Cell Biol 216, 3959–3969.
Pertz O (2010). Spatio-temporal Rho GTPase signaling - where are we now? J Cell Sci 123, 1841–1850.
Pertz OC, Wang Y, Yang F, Wang W, Gay LJ, Gristenko MA, Clauss TR, Anderson DJ, Liu T, Auberry KJ, *et al.* (2008). Spatial mapping of the neurite and soma proteomes reveals a functional Cdc42/Rac regulatory network. Proc Natl Acad Sci USA 105, 1931–1936.
Piper A-K, Sophocleous RA, Ross SE, Evesson FJ, Saleh O, Bournazos A, Yasa J, Reed C, Woolger N, Sluyter R, *et al.* (2020). Loss of calpains-1 and -2 prevents repair of plasma membrane scrape injuries, but not small pores, and induces a severe muscular dystrophy. Am J Physiol Cell Physiol 318, C1226–C1237.
Priya R, Gomez GA, Budnar S, Verma S, Cox HL, Hamilton NA, Yap AS (2015). Feedback regulation through myosin II confers robustness on RhoA signalling at E-cadherin junctions. Nat Cell Biol 17, 1282–1293.
Priya R, Yap AS, Gomez GA (2013). E-cadherin supports steady-state Rho signaling at the epithelial zonula adherens. Differentiation 86, 133–140.
Reyes CC, Jin M, Breznau EB, Espino R, Delgado-Gonzalo R, Goryachev AB, Miller AL (2014). Anillin regulates cell-cell junction integrity by organizing junctional accumulation of Rho-GTP and actomyosin. Curr Biol 24, 1263–1270.
Schindelin J, Arganda-Carreras I, Frise E, Kaynig V, Longair M, Pietzsch T, Preibisch S, Rueden C, Saalfeld S, Schmid B, *et al.* (2012). Fiji: an open-source platform for biological-image analysis. Nat Methods 9, 676–682.
Simon CM, Vaughan EM, Bement WM, Edelstein-Keshet L (2013). Pattern formation of Rho GTPases in single cell wound healing. Mol Biol Cell 24, 421–432.
Sonnemann KJ, Bement WM (2011). Wound repair: toward understanding and integration of single-cell and multicellular wound responses. Annu Rev Cell Dev Biol 27, 237–263.
Stephenson RE, Higashi T, Erofeev IS, Arnold TR, Leda M, Goryachev AB, Miller AL (2019). Rho flares repair local tight junction leaks. Dev Cell 48, 445–459.e5.
Taffoni C, Omi S, Huber C, Mailfert S, Fallet M, Rupprecht J-F, Ewbank JJ, Pujol N (2020). Microtubule plus-end dynamics link wound repair to the innate immune response. Elife 9. https://doi.org/10.7554/eLife.45047
Vaughan EM, Miller AL, Yu H-YE, Bement WM (2011). Control of local Rho GTPase crosstalk by Abr. Curr Biol 21, 270–277.
Vaughan EM, You J-S, Elsie Yu H-Y, Lasek A, Vitale N, Hornberger TA, Bement WM (2014). Lipid domain-dependent regulation of single-cell wound repair. Mol Biol Cell 25, 1867–1876.
Xu S, Chisholm AD (2011). A Gαq-Ca^{2+} signaling pathway promotes actin-mediated epidermal wound closure in C. elegans. Curr Biol 21, 1960–1967.
Yoshida S, Bartolini S, Pellman D (2009). Mechanisms for concentrating Rho1 during cytokinesis. Genes Dev 23, 810–823.
Yüce O, Piekny A, Glotzer M (2005). An ECT2-centralspindlin complex regulates the localization and function of RhoA. J Cell Biol 170, 571–582.
Zhang X, Ma C, Miller AL, Katbi HA, Bement WM, Liu XJ (2008). Polar body emission requires a RhoA contractile ring and Cdc42-mediated membrane protrusion. Dev Cell 15, 386–400.